Optical Microcavities: Single Virus Detection and Nanoparticle Trapping

Frank Vollmer[a] and Stephen Arnold[b]

[a]The Rowland Institute, Harvard University, Cambridge, Massachusetts 02142

[b]MicroParticle PhotoPhysics Lab, Polytechnic Institute of NYU, Brooklyn, New York 11201

ABSTRACT

Single polystyrene nanoparticles are detected from resonance wavelength fluctuations in toroidal and spherical microcavities. The magnitude of the wavelength-shift signal follows a reactive mechanism with inverse dependence on mode volume. By reducing the size of a microsphere cavity we demonstrate sensitivity to single Influenza A virions. Furthermore, we introduce a novel mechanism for trapping and accumulation of nanoparticles at the microcavity-sensor-region by utilizing light-force exerted in evanescent field gradients.

Keywords microcavity biosensor, optical resonance, virus detection, optical nanoparticle trapping

1. INTRODUCTION

Viral infections are a major cause for human disease with potential to rapidly spread through populations across the globe. Early detection of virions is of added urgency in order to prevent a wider outbreak and to improve medical diagnosis and treatment. Rapid virus detection requires a biosensor that ideally responds to a single virus binding event. We demonstrate an optical technique that provides such ultimate sensitivity for detection of label-free virions. Virus and other nanoparticles are detected from resonance wavelength fluctuations in high-Q microcavities where single binding events are discerned from discrete changes in resonance wavelength.

2. NANOPARTICLE EXPERIMENT

To optimize the technique, we first utilize 250 nm-radius polystyrene particles (PS) dissolved at femto-molar concentration in a drop of phosphate buffered solution (PBS) that surrounds a microsphere cavity (Fig. 1). Whispering gallery mode (WGM) resonances are excited in the microsphere by evanescent coupling from a tapered single mode optical fiber[1]. A transmission spectrum is recorded while the wavelength of a distributed feedback laser is tuned across one or more WGMs. The resonance wavelength is determined from the transmission spectrum by locating the minimum of a Lorentzian-shaped resonant line and their [illegible] versus time with ~ 10 ms resolution. The inset in Fig. 1 shows a typical transmission spectrum obtained for a 78 μm-diameter microsphere where resonances are excited by a ~ 763 nm wavelength distributed feedback (DFB) laser. The quality factor is measured ~ 10^6.

Biosensing II, edited by Manijeh Razeghi, Hooman Mohseni, Proc. of SPIE Vol. 7397, 739702 · © 2009 SPIE · CCC code: 0277-786X/09/$18 · doi: 10.1117/12.827264

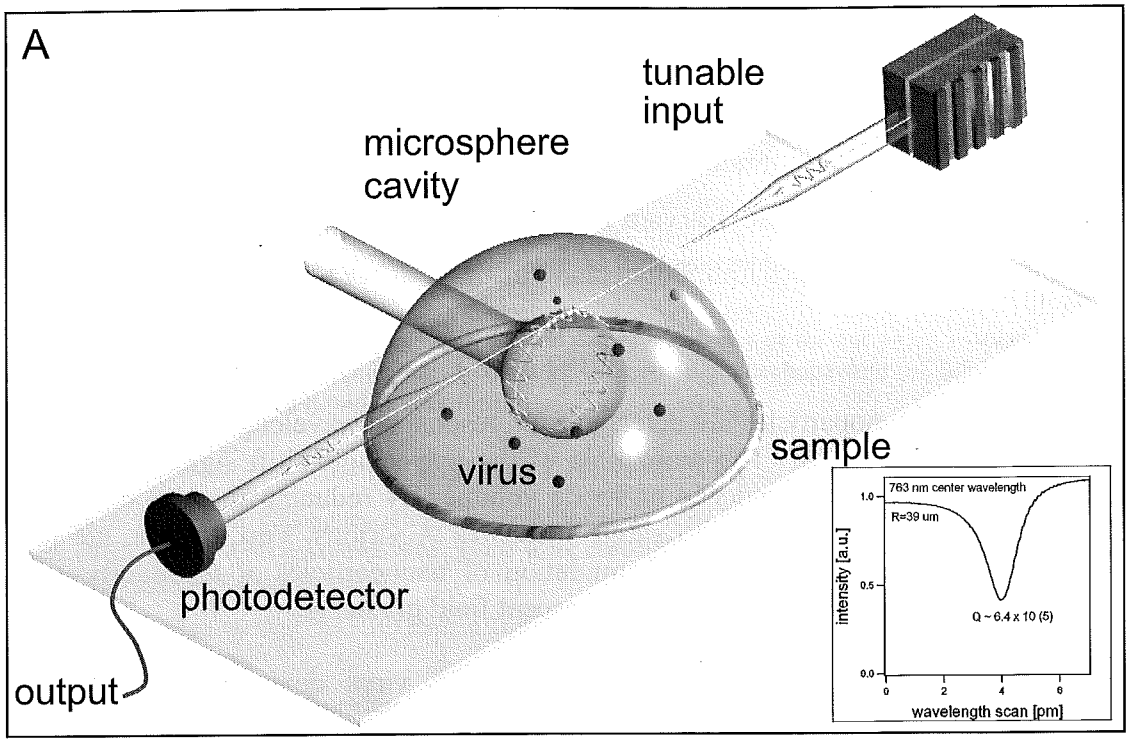

Fig. 1 Experimental setup. Whispering-mode-resonances are excited in the R=39 μm microsphere cavity by using a tunable, distributed feedback laser (here 763 nm nominal wavelength) and by utilizing evanescent coupling from tapered single mode optical fiber. The resonance wavelength is identified by locating the minimum of the Lorentzian-line recorded in the transmission spectrum. The inset shows a typical transmission spectrum with a resonant line ~ 1 pm width corresponding to a resonance quality factor $Q \sim 6.4 \times 10^5$.

Microspheres are fabricated from thinned optical fiber ends that are melted in a focused 10W CO_2 laser. Immediately after its fabrication, the microsphere-on-a-stem structure is mounted on the sample cell and immersed in PBS solution (Fig. 1). The sample cell is enclosed to limit air flow and to stabilize the ambient humidity level as well as temperature. Fig. 2A shows a trace of the recorded fractional resonance wavelength change $\Delta\lambda/\lambda$ for radius a = 250 nm PS particles interacting with a microsphere cavity of radius R ~ 27 μm where resonance is excited at ~ 633 nm wavelength. Spikes of different amplitude are clearly visible against the background cavity noise indicating perturbations (unsuccessful adsorption attempts) by individual PS particles. In Fig. 2A, a single nanoparticle binding and unbinding event is discerned from the step recorded in the wavelength shift signal close to the 300 second time point (binding) and close to the 400 second time point (unbinding). A maximum step height can be distinguished by plotting a histogram of all binding events (not shown).

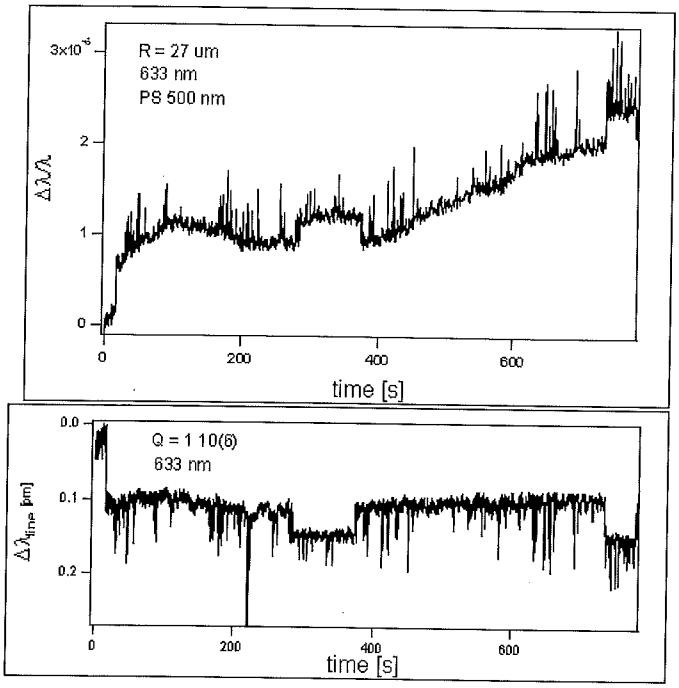

Fig.2 A: Resonance wavelength fluctuations $\Delta\lambda/\lambda$ for radius a = 250 nm PS particles interacting with a microsphere with radius $R \sim 27$ μm. WGM are excited at ~ 633 nm nominal wavelength. B: Simultaneously recorded fluctuations of resonance linewidth. The average Q-factor is measured ~ 1×10^6.

Each wavelength fluctuation induced by a PS nanoparticle is associated with a change in the resonance linewidth (quality Q-factor) due to the scattering induced by the particle. The simultaneously recorded change in linewidth is shown in Figure 2B.

We now direct our experiments toward optimizing the shift signal by reducing microsphere size. We experiment with different-sized microspheres (R = 44 μm – 105 μm) and find a strong dependence of the fractional wavelength shift on the cavity radius[1], scaling as $\sim R^{-2.5}$. As we will see, this is in good agreement with electromagnetic theory associated with single particle reactive WGM sensing, where the largest step heights are predicted for equatorial binding events. In contrast, a $\sim 1/R$ dependence is expected for a shift due to a random surface density[2-4].

3. REACTIVE WAVELENGTH SHIFT

Single particle detection with microcavities relies on the fact that work is done by the evanescent field of a microcavity as the nanoparticle moves from a distant position to the microcavity surface. As a result the energy of light in the resonator is reduced. The frequency of each photon is shifted by $\Delta\omega_r$ in accordance with [2,3]

$$\hbar\,\Delta\omega_r \cong -\frac{\alpha_{ex}}{2}\left\langle E(\boldsymbol{r}_v,t)^2\right\rangle, \tag{1}$$

where $<E(r_v,t)^2>$ is the time average of the square of the field amplitude at the nanoparticle's position r_v due to a single photon resonant state. We have assumed that the nanoparticle is small compared to the wavelength, and has an excess polarizability α_{ex}. By dividing the shift in frequency by the single photon energy $\hbar\omega_r$ on the left and by the volume integral of the associated electromagnetic energy density on the right, we derive a simple expressions for the fractional frequency shift,[2]

$$\left(\frac{\Delta\omega_r}{\omega_r}\right) \cong \frac{-(\alpha_{\mathrm{ex}}/\varepsilon_0)\left|\boldsymbol{E}_0(\boldsymbol{r}_v)\right|^2}{2\int \varepsilon_r(\boldsymbol{r})\left|\boldsymbol{E}_0(\boldsymbol{r})\right|^2 dV}, \tag{2}$$

where $\boldsymbol{E}_0$ is the electric field amplitude, and $\varepsilon_r(\boldsymbol{r})$ is the dielectric constant throughout the cavity. Some insights are arrived at by rearranging Eq.2:

$$\left(\frac{\Delta\omega_r}{\omega_r}\right) \cong \frac{-(\alpha_{\mathrm{ex}}/2\varepsilon_0)}{\int \varepsilon_r(\boldsymbol{r})\left|\frac{\boldsymbol{E}_0(\boldsymbol{r})}{\boldsymbol{E}_0(\boldsymbol{r}_v)}\right|^2 dV}. \tag{3}$$

The first thing which is clear is that although Eqn.3 was constructed by thinking about a single photon state, it applies equally well to multiple photons in the same state, since the square modulus of the field ratio in the denominator is independent of the number of photons. On the right in Eqn.3 there is a ratio of volumes. The numerator is proportional bio-particle-volume V_{bp}, while the denominator will be defined as the sensing-mode-volume V_{sm}. As V_{sm} is reduced in relation to V_{bp}, the shift grows. For a 3D structure such as a microspherical resonator with a particle binding at the equator, one may expect V_{sm} to be proportional to R^3, and therefore provide a large advantage for single nanoparticle detection as the radius is reduced. This insight although approximate, is none-the-less almost correct.

Evaluation of Eqn.2 for a microspherical cavity is most elegantly carried out for a WGM launched around the equator of a glass sphere, as shown in Fig.1. This approach was utilized in Ref.2 for a protein of radius a (~ 3 nm) interacting with the WGM confined to a microsphere of radius R, with the result[2]

$$\left(\frac{\Delta\omega_r}{\omega_r}\right)_s \cong -\frac{\alpha_{\mathrm{ex}}\left|Y_{ll}(\theta,\varphi)\right|^2}{\varepsilon_0(n_{\mathrm{s}}^2 - n_{\mathrm{m}}^2)R^3} \tag{4}$$

where $|Y_{ll}(\theta, \phi)|^2$ is the angular intensity profile describing the "ribbon" of light around the equator for an orbit composed of l waves (i.e. the azimuthal quantum number $m = l$), and n_s and n_m are the refractive indices of the sphere and the external medium, respectively. The WGM interacts with this bio-particle through its evanescent intensity, which extends into the external medium to a characteristic depth L ~200 nm, and drops off exponentially ~ $e^{-(r-R)/L}$. The evanescent length is given by $L \approx (\lambda/4\pi)\,(n_{eff}^2 - n_m^2)^{-1/2}$, where λ is the free space wavelength and n_{eff} is the mode's effective refractive index, which is only slightly below n_s, and will be approximated as n_s for simplicity. In the case of bound protein with a size a much less than L, the exponential factor associated with the slight displacement of the protein's dielectric center from the surface was dropped (i.e. set equal to 1). In the current work although the viral radius a_v ~ 50 nm is small in comparison to L, it is not negligible. As a consequence the shift will be diminished as the ratio a_v/L grows. We account for the displacement of the center of the particle

from the surface by a simple dipole approximation, and obtain the shift by multiplying Eqn.4 by $e^{-a_v/L}$,

$$\left(\frac{\Delta\omega_r}{\omega_r}\right)_s \cong -\frac{\alpha_{\text{ex}}\left|Y_{ll}(\theta,\varphi)\right|^2 e^{-a_v/L}}{\varepsilon_0(n_{\text{s}}^{\ 2}-n_{\text{m}}^{\ 2})R^3}. \tag{5}$$

We clearly see in Eqn.5 the anticipated $1/R^3$ dependence, however it should be noted that if the free space wavelength remains nearly constant as it does in Fig.4, a reduction in microsphere size reduces the number of wavelengths in an orbit, reducing l. The spherical harmonic is sensitive to this; $\left|Y_{ll}(\theta,\varphi)\right|^2$ is proportional to $R^{1/2}$, leaving the shift with a $R^{-5/2}$ dependence.[2] There are some more subtle effects since L extends further into the external medium as the microsphere size is reduced, causing the exponential factor to increase slightly as R decreases.

Eqn.5 may be inverted to obtain the virion radius a_v from a measurement of the maximum shift. This shift occurs for the ribbon mode when the virion binds to the equator ($\theta = \pi/2$) of the microsphere. Only two factors in Eqn.5 depend on the virion radius: the polarizability, and the exponential factor. For sphere-like icosahedral-based virions such as HPV, HSV, HIV or InfA, the polarizability is proportional to the cube of the virion radius (i.e. volume),

$$\frac{\alpha_{ex}}{2\varepsilon_0} = \beta_v a_v^3 \tag{6}$$

with,

$$\beta_v = \frac{4}{3}\pi n_m\left(\frac{dn}{dc}\right)\rho_v$$

where dn/dc is the is differential refractive index associated with adding a mass concentration of virus into aqueous solution, and ρ_v is the mass density of a virus particle. The differential refractive index is known to be fairly constant for protein at 0.18 cm^3/gm, and has been measured for the Tobacco Mosaic Virus (TMV) to be essentially the same. Fortunately virion mass densities fall in a narrow range near 1.2 gm/cm^3, allowing us to estimate $\beta_v \cong 1.2$. For PS particles, β_v can be obtained by modeling them as a homogeneous dielectric spheres ($n_{\text{ps}} = 1.59$) in water, with the result that $\beta_v \cong 1.39$. Since shifts in free space wavelength $\Delta\lambda_r$ are measured experimentally, we will express the maximum value of Eqn.5 (i.e. equatorial binding) in experimental terms,

$$\left(\frac{\Delta\lambda_r}{\lambda_r}\right)_{\text{s, max}} \cong \left(\frac{\beta_v}{\gamma_s}\right)\frac{a_v^3}{R^{5/2}}e^{-a_v/L}, \tag{7}$$

where the factor $\gamma_s R^{5/2}$ in the denominator of Eqn.7 replaces $(n_{\text{s}}^{\ 2}-n_{\text{m}}^{\ 2})R^3/(2\left|Y_{ll}(\pi/2,\varphi)\right|^2)$ in Eqn.5. This replacement is made possible by generating an asymptotic expression for the spherical harmonic in the large l limit, and replacing l in this expression by the resonance condition for the equatorial mode $l = 2\pi R n_{eff}/\lambda_r$, where once again n_{eff} will be approximated as n_s for simplicity. As a result

$$\gamma_s \cong \pi\,(n_s^2 - n_m^2)\left(\frac{\lambda_r}{2n_s}\right)^{1/2}. \tag{8}$$

Since most virions have a radii considerably less than $3L$, one can obtain an approximate solution for the virion radius by moving the exponential function in Eqn.7 to the left and taking the cube root of both sides of the resulting equation. By expanding $e^{+a_v/(3L)}$ to first order, $e^{+a_v/(3L)} \cong 1 + a_v/(3L)$, a linear equation in a_v results, for which the solution is

$$a_v \cong \frac{a_0}{1 - \frac{a_0}{3L}}. \tag{9}$$

where a_0 is

$$a_0 \cong R^{5/6} \left(\frac{\gamma_s}{\beta_v} \right)^{1/3} \left(\frac{\Delta\lambda_r}{\lambda_r} \right)_{\text{s, max}}^{1/3} \tag{10}$$

4. SINGLE INFLUENZA A VIRUS DETECTION

We utilize the knowledge of the reactive sensing mechanism and attempt to increase the wavelength shift magnitude due to single nanoparticles by reducing microcavity size. Furthermore, we optimize the microsphere system for the detection of single Influenza A (InfA) virions. Following this approach, we use tunable laser with at λ ~763 nm wavelength and excite a WGM with Q ~ 6.4×10^5 in R = 39 μm microspheres. We inject InfA virions at concentration of ~10 fM directly into a PBS filled sample cell, since the virions are known to adsorb to silica. The dip-trace of the resonance wavelength $\Delta\lambda_{InfA}/\lambda$ in Fig. 3A reveals clear steps associated with binding of single viral particles. The signal-to-noise ratio ($\Delta\lambda_{InfA}/\Delta\lambda_{noise}$ ~ 3) can be further improved upon by signal processing schemes such as Median filtering. In a second experiment, we label the InfA virus particles with DiIC membrane dye (Invitrogen). Fluorescent images show the binding of InfA particles to the microsphere cavity (Fig. 3B). Surprisingly, we find most of the binding events to localize at the equatorial region of the microsphere cavity where the principal photon energy resides. This observation indicates a novel optical mechanism for trapping and accumulation of nanoparticles by the optical field gradient of a microcavity[5] - and may explain discrepancies for binding rates reported in the literature.

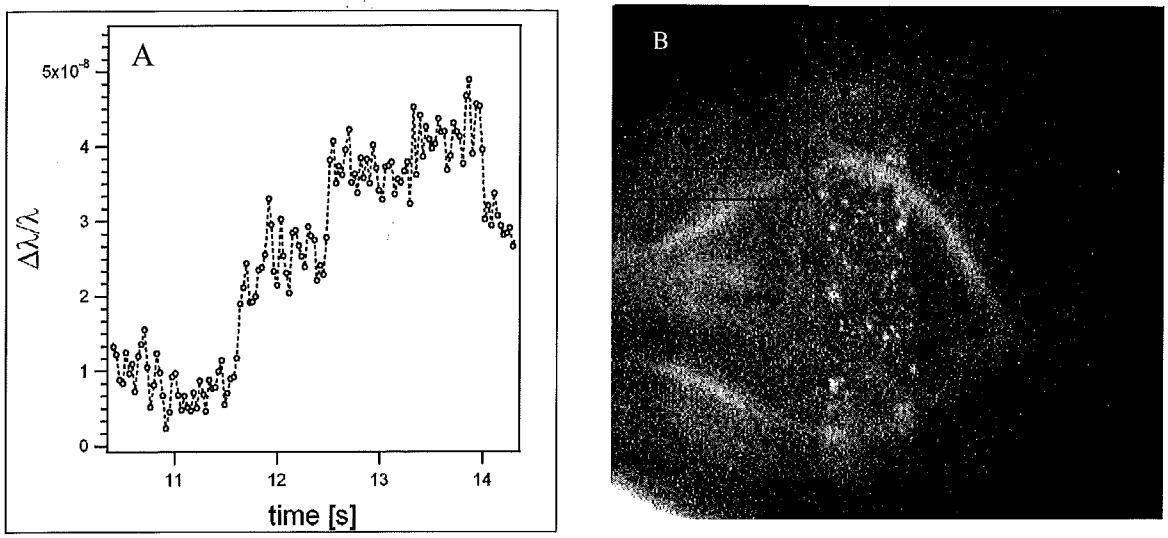

Fig.3 A: Wavelength shift $\Delta\lambda/\lambda$ for Influenza A virus particles. The data was acquired with a microsphere cavity of radius R = 39 μm, and a distributed feedback laser with a nominal wavelength of 763 nm. B: In a second experiment Influenza A virus particles are fluorescently labeled. We image the particles bound to the microsphere cavity using a fluorescent microscope. We observe binding of virions predominantly to the equatorial region of the microsphere cavity, indicating a novel optical mechanism for nanoparticle trapping and accumulation.

5. OPTICAL TRAPPING AND ACCUMULATION OF NANOPARTICLES

A recent paper in Nature Biotechnology[6] has pointed out an unexplained discrepancy in miniature biosensors between theoretical binding rates and experimental results.[1,7] For extremely dilute (sub-femtomolar) solutions the binding delay time calculated based on diffusive and convective transport of target molecules to miniature sensors are impractically long in contrast to recently measured experimental times. A particular example of this discrepancy is the large binding rates (one hundred times larger than estimated in Ref. (6)) of bioparticles to an optical Whispering Gallery Mode (WGM) micro-toroidal bio-sensor.[7] After discussing their convection-reaction-diffusion theory, the authors of Ref. (6) conclude "that additional, yet undetermined ingredients (beyond what we have incorporated here) must be present in the experiments". We have made an observation[5] in the case of spherical and toroidal WGM sensors that an optical mechanism, not discussed in Ref. (6), considerably enhances binding rates. Nanoparticles suspended in aqueous solution are normally in Brownian motion. However, within the reach of the WGM's evanescent field (~ 200 nm) nanoparticles are drawn toward the surface by gradient forces, similar to those present in optical tweezers. The gradient forces draw the nanoparticles towards the high-intensity region of the evanescent field from where they tend to adsorb and accumulate on the surface of the resonator (Fig. 4, example for a toroidal resonator).

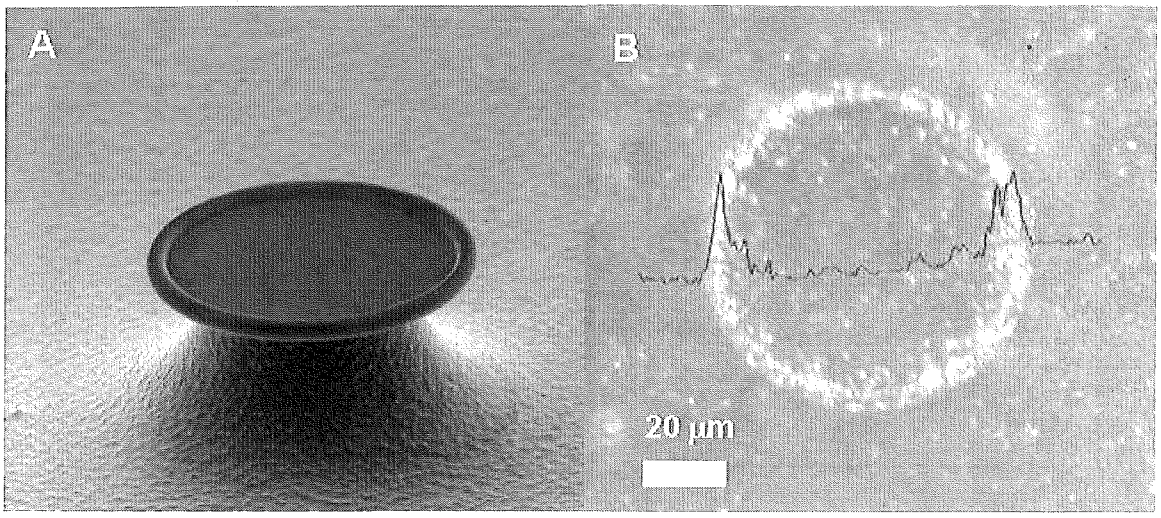

Fig.4 A: Scanning electron microscope image of a ~ 80 μm diameter toroidal resonator. B: Fluorescence image of the same resonator immersed in a solution with 200 nm-diameter polystyrene particles. The nanoparticles are found to bind and accumulated predominantly at the equatorial region of the WGM light orbit. The inset shows grey-scale values averaged for several line-scans taken across the center of the toroid.

In the case of a low binding-affinity or a low density of binding sites, the nanoparticles are propelled around the orbit by radiation pressure[5]. Within this orbital trap, radial stochastic motion is induced by thermal energy within the exponential-potential-well setup by the evanescent field, forcing a nanoparticle to visit the surface many times per micron during its circumnavigation. As a result binding is essentially assured once the nanoparticle is pulled into this stochastic orbit. This considerably increases the binding rate even in the presence of very few binding sites and at extremely low nanoparticle concentrations (fM). In addition the nanoparticle is drawn to the highest intensity of the WGM where its presence produces the largest sensing signal (i.e. wavelength shift). We have been able to successfully model the particles drift speed around the circumference, and the minimum threshold laser power required for orbital trapping[5]. We find that the binding energy W_b is proportion to the product of the resonant quality factor Q and the laser power P. Surprisingly, the threshold power for virus-sized particles is in the one hundred microwatt range due to the build up in intensity caused by the high Q of our WGMs (~ 10^6 -10^7). Thermal energy plays the major combative role in trapping. The trap is secured by raising the binding energy W_b associated with the radial gradient force by a few times the Boltzman energy, k_BT. In the presence of appropriate antibodies at low densities on the surface, the bio-particle binding probability is extremely high. The advantage of this mechanism is that it attracts the particles to the largest intensity within the WGM orbit, which increases their concentration at the place of maximum sensitivity on the resonator surface. The results of this work[5] can add understanding to single molecule detection limits and are applicable for quantitative analysis of the WGM bio-sensor measurements at ultra-low concentrations. The orbital trapping mechanism with high Q WGM sensors is unavoidable considering the low power level at which this opto-mechanical effect occurs. Opto-mechanical forces have already been

demonstrated above optical waveguides for the transport of particles (diameter > 500 nm)[8] at considerable higher laser power levels (~ 50 mW). For WGM biosensors having a Q ~ 10^7 this power level can be reduced by more than 1,000 times, which is expected to make the phenomenon we have described here difficult to avoid.

6. ACKNOWLEDGEMENTS

F.V. was supported by a Rowland Junior Fellowship. S.A. was supported by NSF through the Division of Bioengineering and Environmental Systems, Grant No. 0522668. Address correspondence to vollmer@rowland.harvard.edu.

7. REFERENCES

[1] Vollmer, F. and Arnold, S. "Single Virus Detection from the Reactive Shift of a Whispering Gallery Mode", PNAS 105(52), 20701-20704 (2008).
[2] Arnold, S., Khoshsima, M., Teraoka, I., Holler, S., Vollmer, F. "Shift of Whispering-Gallery Modes in Microspheres by Protein Adsorption", Optics Lett. 28(4), 272-274 (2003).
[3] Vollmer, F., Braun, D., Libchaber, A., Khoshsima, M., Teraoka, I., Arnold, S. "Protein Detection by Optical Shift of a Resonant Microcavity" Appl. Phys. Lett. 80(21), 4057-4059 (2002).
[4] Teraoka, I., Arnold, S., Vollmer, F. "Perturbation Approach to Shift of Whispering-Gallery Modes in Microspheres by Protein Adsorption" JOSA B 20(9), 1937-1946 (2003).
[5] Arnold, S., Keng, D., Shapova, S.I., Holler, S., Zurawsky, W., Vollmer, F. "Whispering Gallery Mode Carousel – a photonic mechanism for enhanced nanoparticle detection in biosensing" Optics Express 17(8), 6230-6238 (2009).
[6] Squires, T.M., Messinger, R.J., Manalis, S.R. "Making it stick: convection, reaction and diffusion in surface-based biosensors" Nat. Biotechnol. 26, 417-426 (2008).
[7] Armani, A.M., Kulkarni, R.P., Fraser, S.E., Flagan, R.C., Vahala, K.J. "Label-free, single molecule detection with optical microcavities" Science 317, 783-787 (2007).
[8] Schmidt, B.S., Yang, A.H.J., Erickson, D., Lipson, M. "Optofluidic trapping and transport on solid core waveguides within a microfluidic device" Optics Express 15, 14322-14334 (2007).